



Biophysical and photobiological basics of water-filtered infrared-A hyperthermia of superficial tumors

Peter Vaupel, Helmut Piazena, Werner Müller & Markus Notter

To cite this article: Peter Vaupel, Helmut Piazena, Werner Müller & Markus Notter (2018) Biophysical and photobiological basics of water-filtered infrared-A hyperthermia of superficial tumors, International Journal of Hyperthermia, 35:1, 26-36, DOI: [10.1080/02656736.2018.1469169](https://doi.org/10.1080/02656736.2018.1469169)

To link to this article: <https://doi.org/10.1080/02656736.2018.1469169>



© 2018 The Author(s). Published with license by Taylor & Francis Group, LLC



Published online: 10 May 2018.



[Submit your article to this journal](#)



Article views: 3236



[View related articles](#)



[View Crossmark data](#)



Citing articles: 6 [View citing articles](#)

Biophysical and photobiological basics of water-filtered infrared-A hyperthermia of superficial tumors

Peter Vaupel^a, Helmut Piazena^b, Werner Müller^c and Markus Notter^d

^aDepartment of Radiation Oncology and Radiotherapy, Klinikum rechts der Isar, Technische Universität München (TUM), München, Germany; ^bMedical Photobiology Group, Department of Internal Medicine, Charité University Medicine, Berlin, Germany; ^cPhysical Optics Consultant Office, Wetzlar, Germany; ^dDepartment of Radiation Oncology, Lindenhofspital, Bern, Switzerland

ABSTRACT

Thermography-controlled, water-filtered infrared-A (wIRA) is a novel, effective and approved heating technique listed in the ESHO quality assurance guidelines for superficial hyperthermia clinical trials (2017). In order to assess the special features and the potential of wIRA-hyperthermia (wIRA-HT), detailed and updated information about its physical and photobiological background is presented. wIRA allows for (a) application of high irradiances without skin pain and acute grade 2–4 skin toxicities, (b) prolonged, therapeutically relevant exposure times using high irradiances (150–200 mW/cm²) and (c) faster and deeper heat extension within tissues. The deeper radiative penetration depth is mainly caused by forward Mie-scattering. At skin surface temperatures of 42–43 °C, the effective heating depth is 15 mm ($T \geq 40$ °C) and 20 mm ($T \geq 39.5$ °C). Advantages of wIRA include its contact-free energy input, easy power steering by a feed-back loop, extendable treatment fields, real-time and noninvasive surface temperature monitoring with observation of dynamic changes during HT, and – if necessary – rapid protection of temperature-sensitive structures. wIRA makes the compliant heating of ulcerated and/or bleeding tumors possible, allows for HT of irregularly shaped and diffusely spreading tumors, is independent of individual body contours, allows for very short ‘transits’ between HT and RT (1–4 min) or continuous heating between both therapeutic interventions. New treatment options for wIRA-HT may include malignant melanoma, vulvar carcinoma, skin metastases of different primary tumors, cutaneous T- and B-cell lymphoma, large-area hemangiomas, inoperable squamous cell, basal cell and eccrine carcinoma of the skin with depth extensions ≤ 20 mm.

ARTICLE HISTORY

Received 26 October 2017
Revised 12 April 2018
Accepted 21 April 2018

KEYWORDS

Water-filtered infrared-A; physics of wIRA hyperthermia; photobiology of wIRA hyperthermia; contact-free hyperthermia; superficial hyperthermia; recurrent breast cancer



1. Introduction

In the *experimental setting*, water-filtered infrared-A (wIRA) has been used since 1991 to assess the impact of localized, contact-free hyperthermia (HT) on therapeutically relevant parameters of the tumor microenvironment (e.g., perfusion, oxygenation status, pH, metabolic status) and intratumor temperature distributions [1–5]. In addition, treatment efficacy of wIRA-HT in combination with fractionated radiation (RT), photodynamic therapy (PDT) [6–9] and thermosensitive, doxorubicin-containing liposomes in a nanomedicine formulation [10] has been documented.

In the *clinical setting*, first promising treatment results along with intratumor temperature measurements upon wIRA exposure for HT treatment were obtained in a preliminary study by Seegenschmiedt [11]. Thereafter, in a prospective multicenter phase I/II study including 53 patients with 58 malignant lesions, Seegenschmiedt et al. [12] have concluded that ‘wIRA can be safely and effectively applied to heat localized, superficial tumors when combined with external beam radiotherapy’.

Using an upgraded, thermographically controlled 2-wIRA-radiator system, Notter et al. [13] have treated large-sized (broad, superficial) heavily pretreated breast cancer recurrences (and re-recurrences) with wIRA immediately followed by hypofractionated RT (5×4 Gy, 1/week). Response rates in this retrospective study were 61% CR and 33% PR, respectively. Local control throughout lifetime after CR of macroscopic disease was 59%. Despite larger tumor sizes and a higher percentage of superficial lymphangitis carcinomatosa, the CR rate was comparable to data published in a recent review by Datta et al. [14]. From this latter systematic review with meta-analysis of combined HT and RT for locoregionally recurrent breast cancer (LRBC) it is concluded that ‘thermoradiotherapy is an efficient and safe palliative treatment option for LRBCs’. Due to the level of evidence, hyperthermia combined with RT has been recommended by current breast cancer guidelines in the USA, in the Netherlands and in Germany [15–19].

In an updated report on 102 patients with recurrent breast cancer, presented during the ESHO-meeting 2017,

CONTACT Professor Peter Vaupel  peter.vaupel@tum.de  Department of Radiation Oncology, Klinikum rechts der Isar, Technische Universität München (TUM), Ismaninger Strasse 22, 81675 München, Germany

© 2018 The Author(s). Published with license by Taylor & Francis Group, LLC

This is an Open Access article distributed under the terms of the Creative Commons Attribution-NonCommercial-NoDerivatives License (<http://creativecommons.org/licenses/by-nc-nd/4.0/>), which permits non-commercial re-use, distribution, and reproduction in any medium, provided the original work is properly cited, and is not altered, transformed, or built upon in any way.

Notter et al. [20] could confirm the data communicated before. In addition, with a higher number of patients, local control throughout lifetime was 73% without any acute grade 2–4 skin toxicities or side effects.

Due to the above mentioned preclinical and clinical data, wIRA has been listed as an appropriate heating technique in the new ESHO quality assurance guidelines for superficial hyperthermia trials [21,22]. In order to assess the special features and the potential of thermographically controlled wIRA as well as the differences to currently used radio- and microwave heating techniques, detailed and updated biophysical and photobiological background information concerning wIRA (together with possible limitations and treatment options beyond breast cancer recurrences) will be presented in this article. The use of wIRA in whole-body hyperthermia is not a subject of this review.

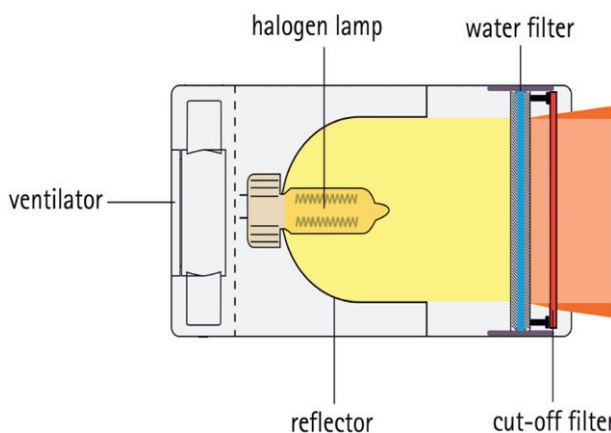


Figure 1. Schematic cross-section of a wIRA radiator (type hydrosun[®] 750, Hydrosun, Müllheim/Baden, Germany). The filament of the halogen lamp is placed in the focal point of a spherical, concave mirror with a radius of 40 mm in order to ideally parallelize the radiation. In practice, radiation leaving the radiator shows a central, homogeneous zone (orange) and a divergent fringe (dark orange) serving as ‘penumbra’ when two radiators are combined.

2. Generation of wIRA for hyperthermia treatment of superficial tumors in the clinical setting

Commercially available technical solutions of wIRA radiators intended for IR-therapy in the clinical setting were developed by Erwin Braun (Frankfurt/Main, Germany) and Manfred von Ardenne (Dresden, Germany) in the 1980s to allow for a high transfer of thermal energy into tissues. Significant spectral parts of unfiltered IR-radiation emitted by conventional IR-lamps are absorbed in the upper tissue layers, mainly by water molecules creating heat pain sensations in the skin, and thus limiting the irradiance necessary to reach therapeutically relevant effects in the oncological setting. The principle of wIRA is derived from tissue heating by solar IR radiation reaching the Earth’s surface, filtered by atmospheric water and water vapor. Water-filtered solar IR radiation formed a crucial environmental condition for the evolution of life on Earth.

In **Figure 1**, a schematic cross-section of the currently used wIRA radiator is shown with a halogen lamp of high correlated color temperature (CCT, about 2900 K), a reflector, a sealed water filter and a cut-off filter to eliminate the visible range <590 nm of emitted radiation [23].

The clinically used wIRA-hyperthermia system (type hydrosun[®]-TWH1500) consists of two wIRA radiators (type hydrosun[®] 750) individually combined with a thermography camera (type Pi450, Optris[®], Berlin, Germany) and a pyrometer for safety control (type CS micro 2 W hs LT15, Optris[®], Berlin, Germany). For real-time surface temperature monitoring of the treated area, all components are parts of a computer-based closed feedback system (see **Figure 2**). Both wIRA radiators can be used individually or combined depending on the size and the surface contour of the target area.

3. Physical basis of wIRA

Electromagnetic radiation with wavelengths between 0.78 μm and 1000 μm is called infrared radiation (IR). According to CIE

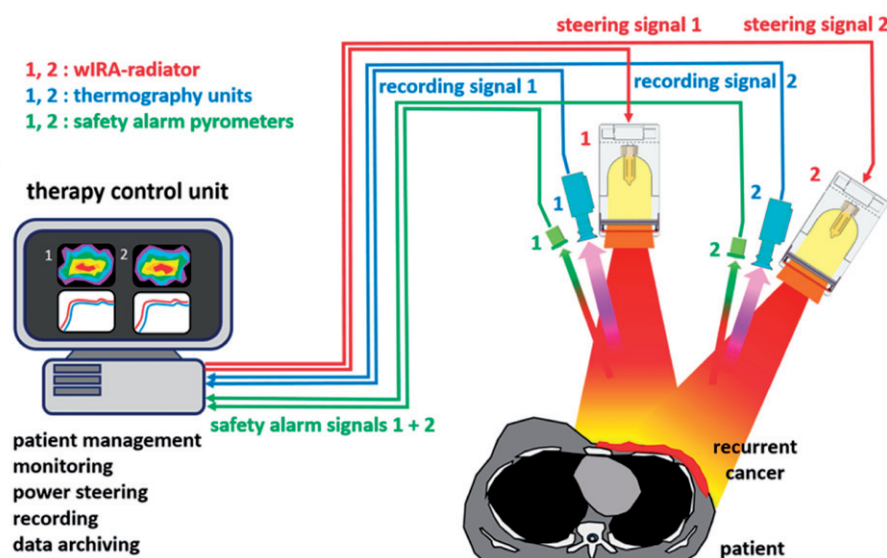


Figure 2. Currently used wIRA-hyperthermia system with two radiators (type hydrosun[®]-TWH1500) to treat large-size (broad, superficial) breast cancer recurrences. Both radiators are steered independently by two thermographic cameras and safety pyrometers.

[24] and DIN 5031/7 [25], this range is divided into three sub-ranges of IR-A (0.78–1.4 μm), IR-B (1.4–3.0 μm) and IR-C (3–1000 μm). These subranges differ from the classification into the subranges of ‘near’ (0.78–3 μm , NIR), ‘mid’ (3–50 μm , MIR) and ‘far’ (50–1000 μm , FIR).

In Figure 3, the emission spectrum of the wIRA-radiator (curve 1), following to a great extent Planck’s radiation law, is compared to the unfiltered spectrum (curve 2) of the halogen lamp (CCT: about 2900 K) in the radiator. This unfiltered spectrum with a maximum at approximately 1000 nm (according to Wien’s displacement law) covers visible radiation, IR-A, IR-B and IR-C, whereas the filtered spectrum is limited to wavelengths between 590 nm and 1400 nm.

The thickness of the water filter of 7 mm was chosen as an empirical compromise between wanted decrease of irradiance within the water absorption bands and unwanted decrease of required irradiance outside these bands. Under these conditions, the water filter abates the irradiance by around 47% at 970 nm, by about 74% at 1160 nm and by almost 100% at wavelengths >1400 nm, whereas the total irradiance for wavelengths between 590 nm and 1400 nm is reduced by only 39%. The optical longpass filter with cut-off wavelength at 590 nm avoids an unwanted major contribution of visible radiation to the IR-A, but allows visual control of the wIRA field.

According to Figure 4, the irradiances used for therapy can be regulated by simply varying the distance between wIRA radiator and patient. Standard distance is 33 cm, controlled by a distance rod. Changing the power supply of the lamp for achieving different irradiances would alter the emitted spectrum according to Wien’s displacement law.

In addition to the spectral distribution, the homogeneity of the irradiance in the treatment area has to be considered. In Figure 5(A), the horizontal distribution of irradiance is presented for different distances between radiator exit and the target field. In the case of curved body contours, incident irradiance decreases by the cosine function of the angle between the direction of the incident radiation and the

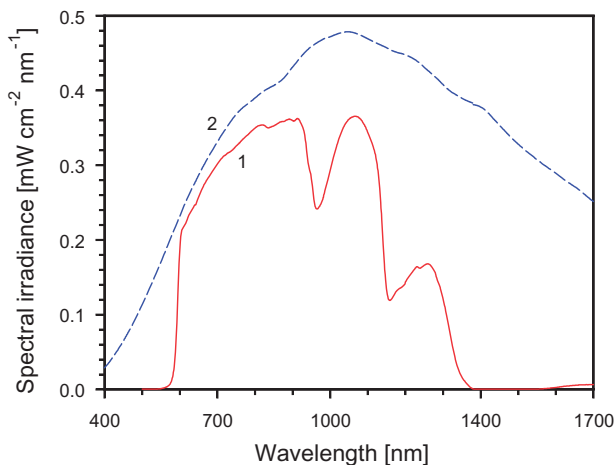


Figure 3. Spectral irradiance of the wIRA irradiator as shown in Figure 1 (type hydrosun[®] 750) as a function of wavelength. Curve 1: With inserted water filter (thickness of the water layer = 7 mm) and a cut-off filter of type BTE 595 (BTE Elsoff, Germany). The spectral output is limited to wavelengths between 590 nm and 1400 nm. Curve 2: Unfiltered halogen radiation (uHR) at about 2900 K CCT. CCT: correlated color temperature.

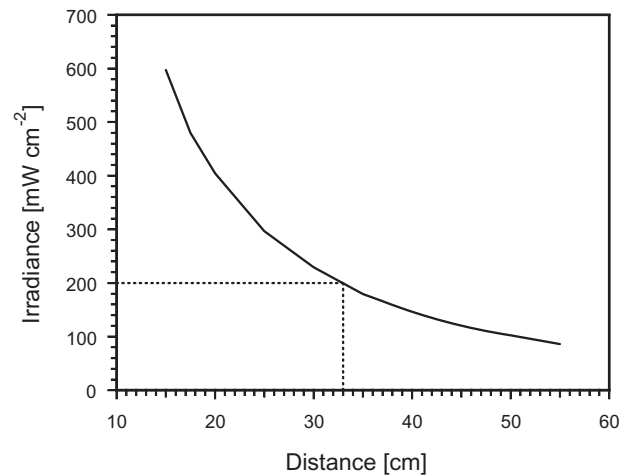


Figure 4. Total irradiance of the wIRA radiator as shown in Figure 1 (type hydrosun[®] 750) equipped with a cut-off filter (type BTE 595; BTE, Elsoff, Germany) as a function of the distance between the radiation exit window and the treatment field. The dotted vertical line indicates the standard distance of 33 cm, the horizontal line the corresponding irradiance of 200 mW cm^{-2} .

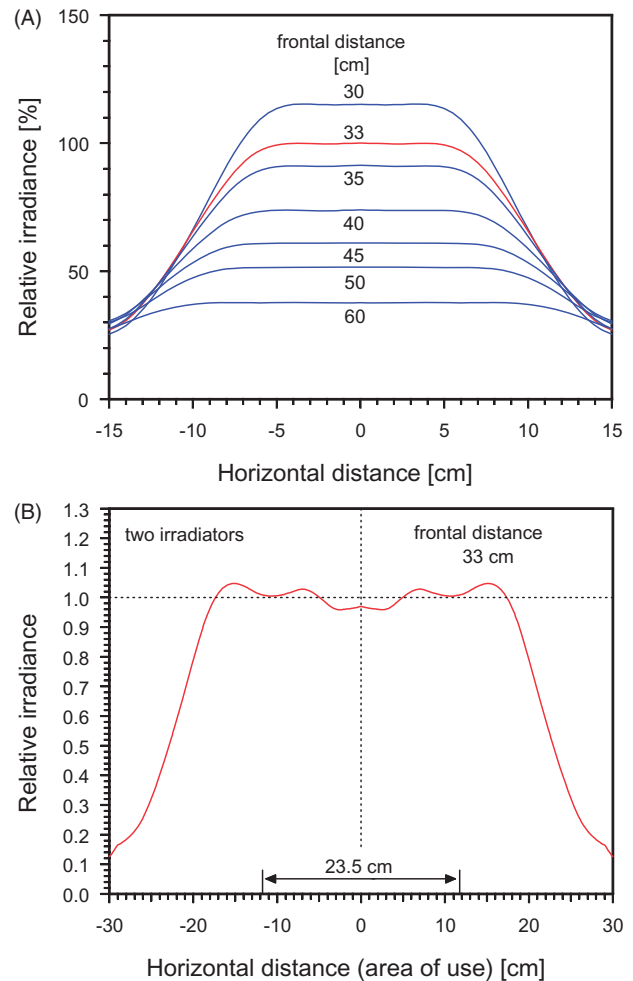


Figure 5. (A) Horizontal distribution of relative irradiance at different (frontal) distances from the radiation exit window, measured for a single radiator (type hydrosun[®] 750). Horizontal distances were referred perpendicular to the optical axis. The distance of 33 cm is recommended for standard applications. (B) Superposition of the radiations of two wIRA-radiators in dependence of their horizontal distance. The optimal distance between the two axes is 23.5 cm. The advantage of the penumbra is allowing such configuration without hot spot.

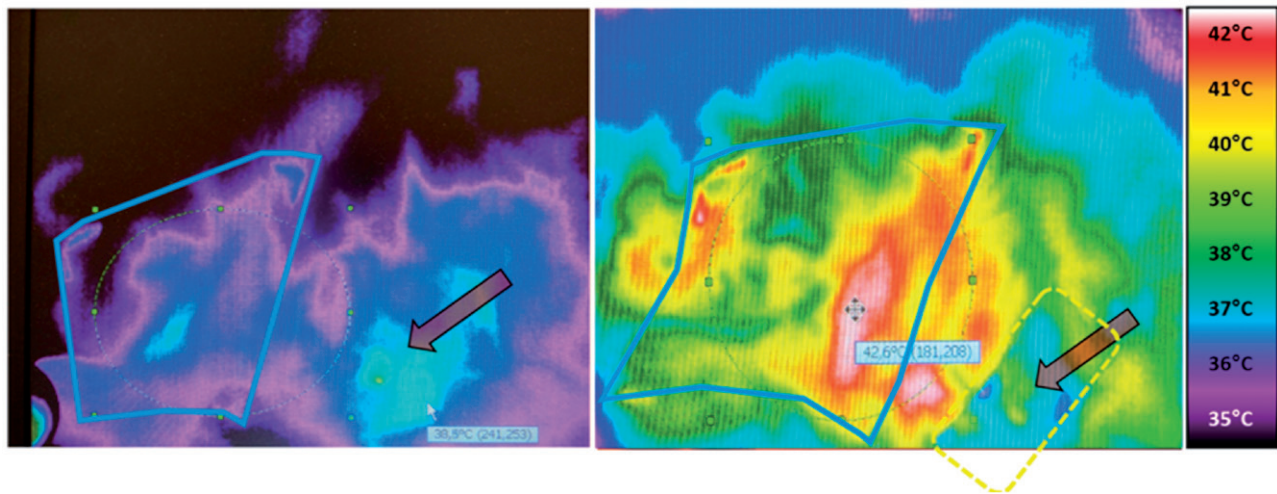


Figure 6. Thermographic control at the onset and during wIRA-hyperthermia. A pigmented senile wart (arrow) was detected early after starting the therapy because of its relatively high absorbance due to chromophores resulting in rapid temperature elevation. In order to avoid its influence on the power steering, the wart was protected with tape, so that heating of the region of interest was no more disturbed. Treated region with field marks is indicated by the solid line; broken rectangle depicts the area protected with tape.

normal to the anatomical contour. For clinical reasons, the circular radiation field of a single radiator has intentionally no sharp margin in the periphery. This penumbra (as shown in Figure 1) allows for an overlapping of the radiations of two radiators concurrently used in cases of broad lesions and/or varying contoured anatomies (see Figure 5(B)). The optimal distance between the two radiators can be assessed by real-time thermography. Furthermore, the two radiators can be adjusted in different angles according to individual requirements of the treatment field. The use of real-time thermographic imaging has the advantage that maladjustment of the radiators can be detected in the thermographic image and, if necessary, be corrected at the onset of therapy. During the treatment, the location of maximum skin surface temperature is indicated by crosshairs. It is up to the physician's decision to cover this spot, e.g., by a tape (Figure 6).

The temperature of the hottest spot within the entire radiated field captured by the IR-camera is compared to the pre-selected maximum temperature permitted, and steering is done accordingly: heating is interrupted when the upper threshold (e.g., 43°C) is reached and is switched on when the maximum surface temperature falls below the lower threshold (e.g., 42°C). Possibly occurring 'cold spots' are at present not compensated due to technical reasons.

Notably, the extension of the therapeutically heated tissue area is definitely larger than the diameter of the maximum relative irradiance due to lateral heat dissipation as a consequence of convection and conduction.

4. Photobiological basis of tissue heating by wIRA

Human tissues are optically turbid media with several interactions of IR radiation with cutaneous/subcutaneous tissue characterized by different physical processes: (a) *reflection* at the surface, (b) *refraction* at interfaces (e.g., air/skin or variable tissue densities), (c) *absorption* by water molecules and chromophores, (d) *scattering* (forward and back), and (e) *re-emission* (as a consequence of backscattering).

The main absorbents for wIRA are water molecules (water content of most soft tissues: 65–70%), and chromophores such as heme proteins, pigments and certain lipids. In general, tumors have a higher water content (on average +10% v/v) than the surrounding normal tissue/tissue of origin [26–28] causing a higher radiative absorption by the tumor (i.e., leading to a better heating) compared to normal tissues.

There are two kinds of scattering: (a) *Rayleigh-scattering* for scatters with diameters 1/100–1/20 smaller than the wavelengths, and (b) *Mie-scattering* for diameters in the order or exceeding the wavelengths. Assuming a mean wavelength in the wIRA spectrum of 900 nm, cell membranes (6–10 nm), the cytoskeleton (5–25 nm) and ribosomes (10–20 nm) will induce Rayleigh-scattering. Since most structures such as muscle fibers (5–150 μm), cell nuclei (5–16 μm), mitochondria (1–5 μm) and other intracellular organelles, and collagen fibers (approx. 1 μm) are much larger, they induce forward oriented Mie-scattering, which is by far dominating.

Further sources for scattering may be fluctuations of the dielectric constant, of densities and concentrations, and of the refractive index as well. Rayleigh-scattering supports isotropic distribution of radiation, whereas Mie-scattering preferentially leads to forward orientation. All processes mentioned are responsible for the attenuation of the incident irradiance. They also depend on the wavelength and on the special composition of target tissues (i.e., content of relevant chromophores and scattering centers).

Photon energy of wIRA in tissue is mainly converted into kinetic energy of water molecules, perceived as heat. But energy can also be absorbed by photoacceptors causing photochemical processes that mean nonthermal reactions. These latter effects are based on a direct stimulation of cells or cell structures (e.g., cell protrusions, influence on cytochrome c oxidase, neurostimulation, wound repair and cell protection (reviewed in [29]). In order to detect nonthermal effects, dermal fibroblasts have been exposed to wIRA-radiation without warming up the cells [30]. The authors did not observe any impact on vital cell processes but identified a

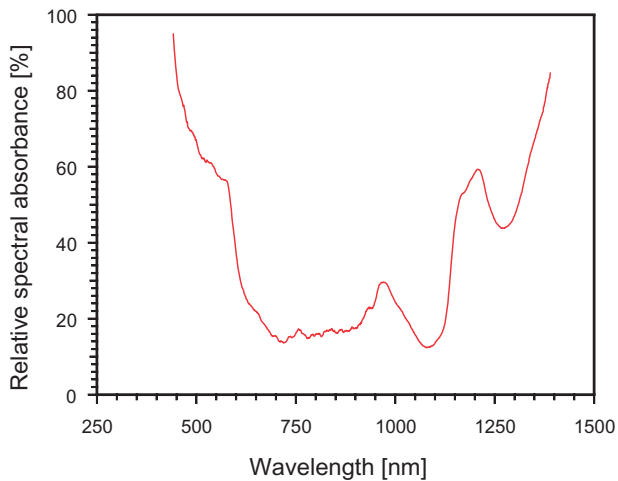


Figure 7. Relative spectral absorbance of radiation (visible light + wIRA) as a function of wavelength measured *in vivo* in human soft tissue (ear lobe) at a depth of 2.4 mm (fair skin). Data calculated from direct measurements of spectral remittance and transmittance [38].

nonthermal DNA-protective effect (i.e., a less pronounced DNA damage upon a subsequent UVB exposure). Piazena et al. [31] have shown that wIRA exposure did not generate measurable cell death or inflammation in the tissue even if an irradiance of 190 mW cm^{-2} within 780–1400 nm (equivalent to 240 mW cm^{-2} within 590–1400 nm) was applied during a treatment time of 30 min. Moreover, only convective heating by air flow, but not heating by wIRA increased significantly the number of free radicals in skin. Safety aspects of the use of wIRA in the experimental and clinical setting have been described in detail (e.g., [29,32–35]). From these reports it is concluded that the application of wIRA with adequate irradiances is a safe procedure. In the clinical setting, wIRA has widely been used in various nononcological therapeutic applications since the early 1990s in daily routine as well as in randomized clinical trials [e.g., in wound healing, reviewed in [36]] without any wIRA-related toxicity. wIRA is also employed in incubator nursing and primary care of pre-term neonates [37].

4.1. Radiative penetration depths and absorption of wIRA in the tissue

The spectral range of wIRA matches the range of the so-called ‘optical window’ of living tissues where absorption of radiation is small (see Figure 7).

As most of the soft tissues contain 65–70% water, reduction of the irradiance within the water bands and elimination of IR-B and IR-C is a main condition for energy deposition in the subcutis and for preventing heat pain and thermal skin damage. In Figure 8, the characteristics of radiative interaction of wIRA compared to the unfiltered halogen lamp radiation (uHR) are calculated for fair human skin [35,38,39] and verified for wIRA by direct *in vivo* measurements [38].

In Figure 8(A) the losses of the incident irradiance by re-emission and reflection at the skin surface are: 43% for wIRA and 16% for uHR. The remaining wIRA irradiance penetrating the tissue decrease to 50% at a depth of 0.5 mm, to 36.79% ($=1/e$) at 1.3 mm, to 10% at 5 mm, and to 1% at 15 mm

[35,38] (curve 1). The corresponding data for the uHR are 36.79% ($=1/e$) at 0.5 mm, 10% at 2.6 mm and 1% at 9.3 mm (curve 2) [39].

Figures 8(B,C) provide characteristics of absorption in the tissue for both radiations. Here, the ‘sub-surface’ irradiance (which is defined as the part of the incident irradiance remaining for penetration after re-emission and reflection) was set to 100% at a ‘depth’ of 0 mm for realistic comparison. As shown in Figure 8(B), about 10% of sub-surface wIRA-irradiance is absorbed between the skin surface and the upper dermis at a depth of 0.3 mm. In contrast, uHR is already absorbed at a depth of 0.06 mm. Cumulative absorbance increases to about 50% for wIRA at a depth of 2 mm, for the unfiltered halogen radiation at a depth of 0.4 mm. Finally about 1% of wIRA reaches a depth of 16.8 mm, whereas the unfiltered halogen radiation ends at a depth of 10 mm [35,38,39]. Figure 8(C) presents the vertical profiles of relative absorbance in the tissue for wIRA and uHR which were calculated by differentiation of the data shown in Figure 8(B) using depth steps of 0.1 mm. The relative absorbance of the sub-surface irradiance within the epidermis (0.1 mm) is about 3.2% for wIRA (curve 1) and approximately 16.6% for uHR (curve 2). At the interface skin/subcutis both radiations show the same relative absorbance of about 2.3%. However, with increasing depth, the relative absorbance decreases to about 0.01% at 20 mm for wIRA, and at 13.8 mm for uHR [35,38,39]. In Figure 8(D) the depth profiles of the ratio ‘sub-surface irradiance of wIRA/sub-surface irradiance of uHR’ (curve 1) and of the ratio ‘relative absorbance of wIRA/relative absorbance of uHR’ (curve 2) are depicted. From these data it is obvious that (a) sub-surface irradiance of wIRA progressively exceeds that of uHR with increasing depth. Starting with a value of 1 at sub-surface (depth = 0 mm), the ratio increases up to 2.4 at the interface skin/subcutis (depth = 1 mm) and reaches a value of 5.7 at a depth of 20 mm; (b) relative absorbance of unfiltered radiation significantly exceeds that of wIRA in the skin for depths ≤ 1 mm. In contrast, the relative absorbance of wIRA progressively exceeds that of uHR in the subcutis up to a factor of 5.35 at a depth of 20 mm.

Due to these features, it is obvious that wIRA is more effective for heating of subcutaneous tissue than uHR or IR-C radiation, the latter being completely absorbed in the epidermis [39]. Moreover, wIRA can reach blood vessels effectively within the range of the above mentioned penetration depths and, therefore, can transfer radiative energy into the circulating blood. Consequently, wIRA allows for the application of (a) prolonged therapeutically relevant exposure times using approximately two-times higher irradiances without causing pain [39] and severe skin toxicities [13] (200 mW/cm^2 versus $<100 \text{ mW/cm}^2$ uHR, the so-called ‘conventional IR-A’), and (a) faster and deeper heat extension within (tumor) tissues [38].

First comparisons of the heating properties between wIRA and uHR on human tissues have already been performed by Vaupel et al. with a prototype of the wIRA radiator [40,41]. Specific absorption rates (SARs) and flow rates derived from these early measurements with the prototype wIRA radiator according to the equations presented in section 4.2 are shown in Table 1. These data confirm the statements made

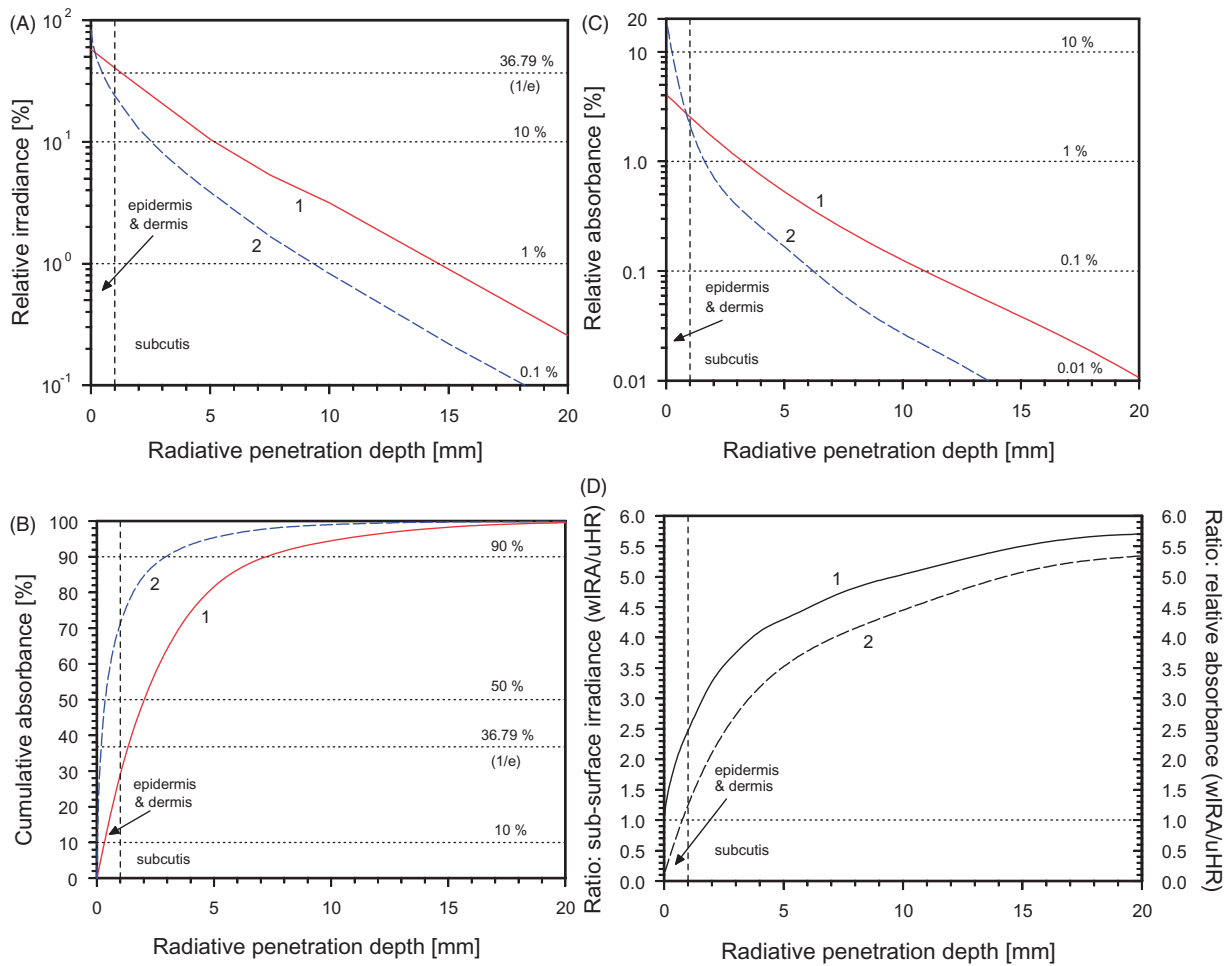


Figure 8. Optical characteristics of wIRA compared to the unfiltered halogen radiation (uHR). Data are calculated for fair skin assuming a plane parallel interface between air and skin and local invariance of the spectral coefficients of absorption and scattering, and of the refractive index [35,38,39]. In panels A–C curve 1 represents wIRA, curve 2 shows uHR data. (A) Relative irradiance penetrating into tissue as a function of depth. (B) Cumulative absorbance as a function of tissue depth. (C) Relative absorbance as a function of tissue depth. Results are calculated by differentiation of the integral data in B using depth intervals of 0.1 mm. (D) The ratio of the penetrating (sub-surface) irradiances (curve 1) and the ratio of relative absorbances (curve 2) between wIRA and uHR as a function of depth.

Table 1. Specific absorption rates (SAR) and flow rates derived from invasive temperature measurements in skin and subcutis of the lumbar region of human subjects during thermotherapy using the prototype wIRA radiator and thermographic control of the skin surface temperature [40].

	SAR [mW/g]	Flow rate [$\text{ml} \times \text{g}^{-1} \times \text{min}^{-1}$]
wIRA		
Subepidermal layer	42.6	0.075
Subcutis (depth ≈ 1 cm)	17.4	0.060
uHR		
Subepidermal layer	55.4	0.083
Subcutis (depth ≈ 1 cm)	14.8	0.058

Energy deposition in the subepidermal layer is higher by uHR, whereas wIRA transfers more energy into the subcutis. The flow rates calculated are in accordance with experimental data published earlier.

above. It is obvious that energy deposition in the subepidermal layer is higher by uHR, whereas wIRA transfers more energy into the subcutis. The flow rates calculated are in accordance with experimental data published earlier.

4.2. Calculation of SAR values and estimates of perfusion rates in normal skin and in recurrent breast cancers

Using initial power-on tissue temperature transients obtained with the currently used TWH1500 system, SAR values related

to different tissue depths have been calculated upon wIRA-heating with an irradiance of 200 mW/cm^2 , using the formula: $\text{SAR} = c \times \Delta T / \Delta t$, where c denotes the specific heat capacity of the tissue and ΔT the local temperature increase during the exposure time Δt . For c , a mean value of 3.6 Ws/g K was chosen according to Wust [42]. The following data were obtained:

Subepidermal layer: 81 mW/g , outer tumor layers: 81 mW/g , lymphangitis carcinomatosa: 77 mW/g , tumor/scar interface: 83 mW/g , recurrent breast cancer (at a depth of approximately 2 cm): 29 mW/g . These values are in agreement with data described for ‘effective heating’ [42]. In these cases the heating-up rates were 0.5 K/min . Flow rates (FR) were calculated based on the above SAR values using the empirical formula $\text{FR} = 0.015 \times \text{SAR} / \Delta T$ [42]. ΔT defines the local temperature increase ranging from about 7 K in the subepidermal layer to about 3 K at a tissue depth of 20 mm. The respective values are as follows: normal subcutis $0.17 \text{ ml g}^{-1} \text{ min}^{-1}$, outer tumor layers $0.21 \text{ ml g}^{-1} \text{ min}^{-1}$, and recurrent breast cancer tissue $0.13 \text{ ml g}^{-1} \text{ min}^{-1}$. These calculated flow rates are comparable with mean flow values published earlier for breast cancers ($\text{FR} = 0.20 \text{ ml g}^{-1} \text{ min}^{-1}$ [43,44]) and for the normal skin ($\text{FR} = 0.13 \text{ ml g}^{-1} \text{ min}^{-1}$ [45]).

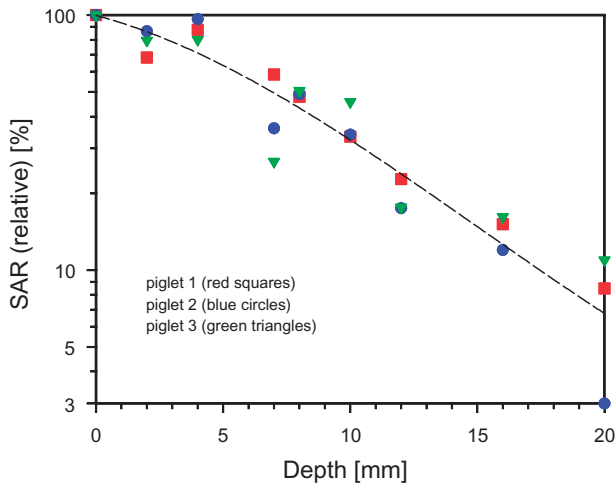


Figure 9. SAR data as a function of tissue depth in three anaesthetized piglets exposed to wIRA using incident irradiances of 139 mW cm^{-2} (piglet 1) and of 113 mW cm^{-2} (piglets 2 and 3).

In order to get a comprehensive view with high time-, temperature- and depth-resolution on the formation of the heated tissue volume during wIRA exposure, anaesthetized piglets have been irradiated with different irradiances. In **Figure 9**, relative SAR values related to the depth in the tissue upon wIRA exposure are depicted (data derived from invasive temperature measurements). The values decrease from 100% (about 96 mW/g for an incident irradiance of 139 mW/cm^2 , and about 62 mW/g for an incident irradiance of 113 mW/cm^2) in the upper epidermis to about 35% at 10 mm depth, and approximately 8% at 20 mm tissue depth.

4.3. Therapeutically relevant tissue/tumor temperatures in wIRA-hyperthermia and effective heating depths

Minimum tumor temperatures of 39°C [46] or 40°C [21] and sufficiently homogeneous temperature distributions in the treatment field are prerequisites for effective hyperthermia treatment in the oncological setting.

Possible factors influencing the temperature distributions in the target field/volume are (a) incident irradiance and its temporal variation during the exposure, (b) duration of the exposure, (c) homogeneity of the incident irradiance, (d) size of the treatment field, (e) physiological variations in the body contour (plane vs. strongly curved), (f) skin surface patterns (surface irregularities, pigmentation, perspiration, superficial blood vessels, scars, ulcerations and bleeding, hornification), (g) heterogeneity in tissue composition (e.g., vascularity, fat and muscle layers, water content, edema formation), (h) spatial and temporal heterogeneities in blood flow and interstitial fluid pressure, and (i) effectiveness of stimulated counter-regulatory mechanisms upon heat load (within a single treatment and/or during the treatment schedule). From this compilation of possibly influencing factors it is evident that heterogeneities in tumor temperatures cannot be avoided in most cases.

Figure 10(A) shows that individual factors such as variability in thermoregulation may result in inter-individual differences in skin surface temperatures (decreases) during the IR

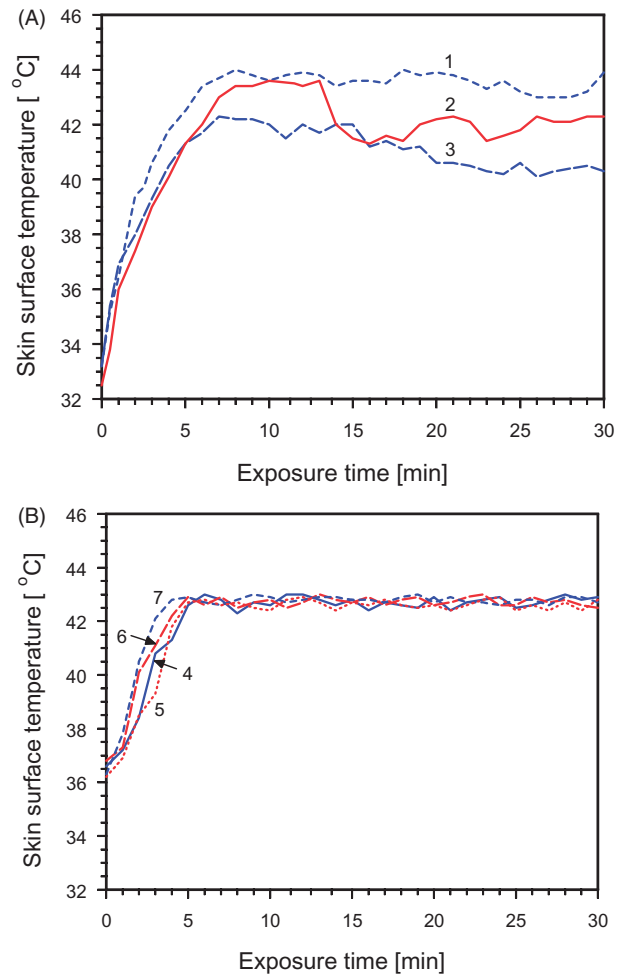


Figure 10. Skin surface temperature as a function of exposure time using a wIRA irradiance of 200 mW cm^{-2} . (A) Temporally constant exposure of the backs of three healthy volunteers (1–3) without temperature control. (B) Controlled skin exposure by switching on/off according to the thermographic feedback signal (see **Figure 2**). In different treatments measurements were taken on normal skin (4), on lymphangitis carcinomatosa (5), on tumor tissue (6) and on tumor/scar tissue (7). Initial skin surface temperature of patients was slightly elevated due to activities in preparation of the treatment. No air ventilation, room temperature $22\text{--}24^\circ\text{C}$.

exposure even if the same irradiance is applied and the environmental conditions are identical. These unwanted effects, which may counteract the efficacy of treatment, can be avoided by the thermography-based feedback system for simultaneous control of the skin surface temperature as described above. This is shown in **Figure 10(B)**. Maximum skin surface temperature of all patients increased up to approximately 43°C within less than 5–6 min after starting exposure as required by the ESHO guidelines [22]. Moreover, maximum skin surface temperatures were maintained between 42.5 and 43°C during the whole treatment session according to the therapeutic schedule and in order to prevent heat pain and burns [47,48].

In tissues below the body surface, temperatures in general decrease with depth (see **Figure 11**). At steady-state surface temperatures of 42°C , tissue temperatures $\geq 40^\circ\text{C}$ were assessed up to a depth of approximately 15 mm, temperatures $\geq 39^\circ\text{C}$ up to a depth of about 30 mm [12,13,49]. In cases of restricted convective transport or if fat tissue layers reduce conductive heat transport, tissue temperatures may

slightly exceed skin surface temperature (see Figure 12). This phenomenon may enhance the therapeutic efficacy of wIRA in superficial tumors. The safety control system interrupts wIRA-radiation at 43 °C maximum skin surface temperature, giving enough safety scope to reliably avoid thermal skin damage which may occur at temperatures >45 °C.

5. Validation of wIRA-heating using phantoms

First measurements of heating properties of wIRA using phantoms were performed by Krüger et al. [50] and Seegenschmiedt [11]. In these earlier studies, agar phantoms were used initially prepared for microwave frequency heating (e.g., 433 MHz and 915 MHz, equivalent to wavelengths of 69 cm and 33 cm). In contrast, the wIRA spectrum comprises frequencies between 3.80×10^8 MHz and 2.14×10^8 MHz, equivalent to wavelengths of 780 nm and 1400 nm.

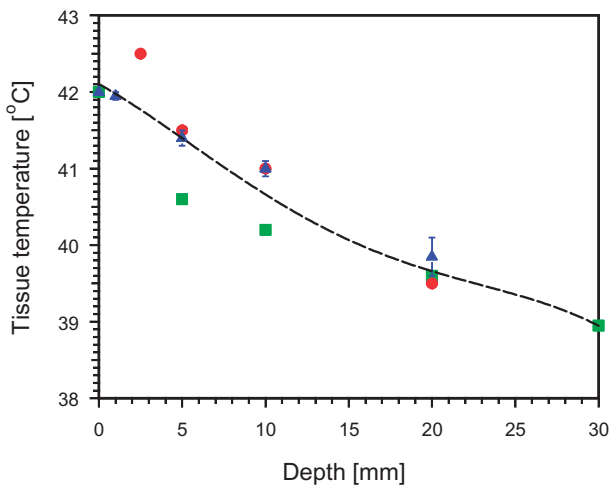


Figure 11. Mean temperature profile during wIRA exposure under steady-state conditions. Measured data in normal tissues [49] (open squares), tumor tissues [12] (open circles) and in recurrent breast cancers [13] (solid triangles).

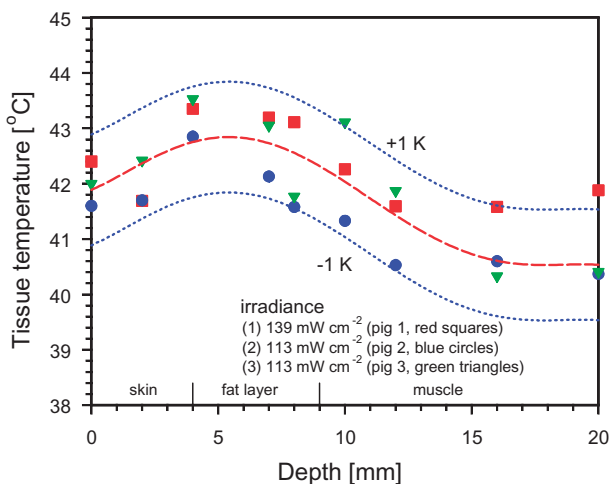


Figure 12. Mean tissue temperature profile upon 30 min wIRA exposure of three anaesthetized piglets (see Figure 9). Thickness of the skin: 4–5 mm, thickness of the fat layer: approx. 5 mm. The maximum tissue temperature exceeded surface skin temperature by about 1 K. Inter-individual variability of tissue temperature was in the range of ± 1 K. Room temperature: 22–24 °C (no air ventilation).

The relevant parameters for radiation in the microwave range are electric conductivity and dielectric permittivity. Both parameters can be derived from Maxwell's electromagnetic theory. As already mentioned above (see Section 4), besides absorption, especially Mie-scattering has to be considered, since the more forward oriented Mie-scattering is dominating with increasing cellular and extracellular structures. This leads to completely different requirements for a tissue-equivalent wIRA-phantom. Components of the phantoms used so far (e.g., sugar, electrolytes and agar) are completely dissolved or suspended in water without any contribution to scattering. To account for scattering, a novel phantom has been used based on the recipes of Luaidi et al. [51]. Accordingly, the components of the phantom were chosen in a way that the absorption coefficient μ_a and the scattering coefficient μ_s coincide with the values for muscle tissue at 900 nm, which is almost in the middle of the wIRA-spectrum. Basic materials were a two-component silicon, aluminum oxide powder (Al_2O_3) and a cosmetic powder containing titanium oxide particles.

In order to monitor wIRA-induced heating of this novel phantom, a thermography camera (VarioCAM hr head 400, Infra Tec, Dresden, Germany) was used [52]. To assess correct absolute temperature readings, the emission coefficient of the phantom was measured ($\varepsilon = 0.91$ at 40 °C), allowing for direct data collection from the entire phantom surface.

- a. *Vertical temperature profiles* exhibited a temperature rise of 9.6 K at 1 cm depth within 6 min as using an irradiance of only 92 mW/cm² (Figure 13, curve B). Choosing the recommended irradiance of 200 mW/cm², the respective temperature rise is 20.8 K, thus exceeding the minimum temperature increase (as required by ESHO [22]) by a factor 2.2 (Figure 13, curve A). Under these conditions, the thermal effective penetration depth (TEPD) as defined by ESHO [22] was determined as 9.0 mm. For these temperature measurements, the

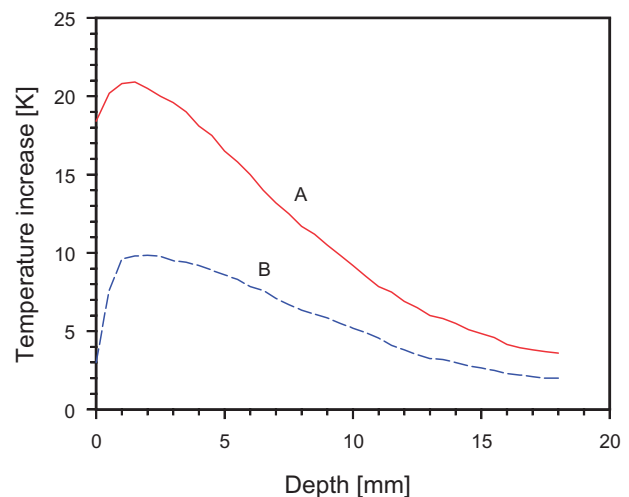


Figure 13. Temperature increase as a function of depth in a "wIRA-phantom" upon 6 min of exposure. Curve A: Incident irradiance 200 mW/cm², corresponding to the standard distance of 33 cm between radiator and phantom surface. Curve B: Incident irradiance 92 mW/cm², corresponding to a distance of 53 cm between radiator and phantom surface (for details see also Figure 4). Phantom temperature before wIRA exposure: 22.5 \pm 0.2 °C (no air ventilation).

phantom was divided along a vertical plane into two halves, so that the depth of maximum temperature increase could be assessed.

- b. *Lateral temperature profiles* were measured after 6 min heating time on the surface only because sufficiently thin slices of the phantom could not be manufactured without significant technical efforts. In larger depths, however, lateral temperature profiles can be estimated by vertical temperature profiles distributed over the entire cross-section, leading to a number of widely overlapping profile lines with high temperatures (see Figure 14) indicating a homogeneous heating of the phantom. This pattern can also be verified by the lateral temperature profiles shown in Figure 15. The corresponding

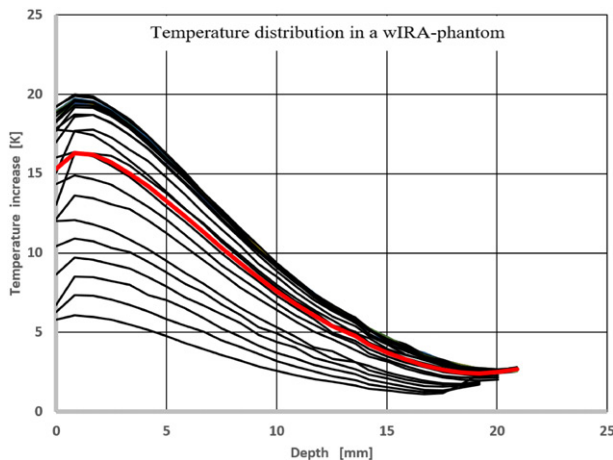


Figure 14. Vertical temperature profiles distributed across the entire cross-section with averaged depth temperature curve (bold). Standard distance between radiator and phantom surface: 33 cm, heating time: 6 min.

Lateral temperature distribution at the surface of a “wIRA-phantom”

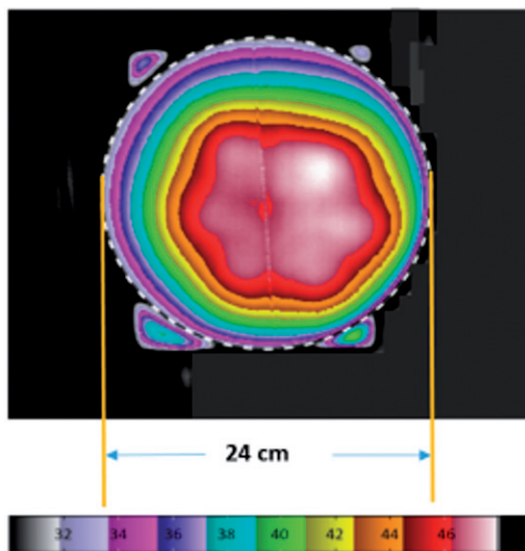


Figure 15. Lateral temperature distribution at the surface of the ‘wIRA-phantom’. The phantom edge is marked by the dotted line. Phantom height: 2 cm, heating time: 6 min. Slight asymmetries are caused by suboptimal positioning of the wIRA-radiator. The corresponding effective field size (EFS) according to the ESHO guidelines is determined to about 300 cm², which equals a circular area with a diameter of 19.6 cm. The minimal temperature increase on the entire phantom surface is 5.0 K.

measurement was performed in the standard distance after a heating time of 6 min.

6. Thermometry and thermal imaging

Temperature assessment based on IR-radiation measurements (e.g., IR-camera, IR-thermometer) is in general not suitable to assess absolute values. To overcome this problem, a high-quality black radiator and thermometers measuring absolute values are currently used. The absolute temperature at a defined reference point within the treatment field can be measured with subsequent readjustment of the respective emission coefficient in the IR-camera/IR-thermometer, and thus correcting the temperature reading.

In case of nonmalignant, heavily pretreated tissues microwave hyperthermia [53] as well as wIRA hyperthermia *without temperature control* can induce burns by overheating due to disturbances of the microcirculation and other factors. Seegenschmiedt et al. [12] have reported skin reactions upon wIRA exposure which required the immediate termination of further heating.

Integrating the IR-camera into the closed feedback system allows for (a) automatic shut-off and switch-on functions limiting the maximum surface temperature to 43 °C and thus preventing any thermal skin damage, (b) contact-free assessment of large surface temperature distributions, (c) observation of dynamic developments during heating sessions, (d) instant and easily achievable protection of heat-sensitive structures (e.g., scars).

7. Conclusions

wIRA for hyperthermia treatment of superficial tumors is a unique technique in the oncological setting since it uses – for the first time – a contact-free energy input and allows for real-time temperature monitoring of dynamic changes in the treatment field. Therefore, patients do not suffer from body restrictions by boluses/applicators or painful contact with ulcerated lesions. The risk of acute thermal skin damage is substantially reduced, even in heavily pre-treated breast cancers. At maximum skin surface temperatures of 42–43 °C, the effective heating depth is 15 mm (≥ 40 °C) and 20 mm (≥ 39.5 °C), respectively. wIRA is a novel, approved and clinically effective technique [54].

8. Outlook

Although the oxygenation status of recurrent breast cancers is substantially poorer than in the primary tumors [55–57] and O₂ tension distributions of tumors growing in formerly irradiated tissue are distinctly shifted to more hypoxic values [58] (i.e., with an increasing number of radioresistant cancer cells and an escape from antitumor immune responses), and also considering possible further decreases of the mean pO₂ values after hyperthermia [59], good local control through lifetime after CR of macroscopic disease can be achieved with wIRA combined with hypofractionated RT with this effective treatment option.

Due to its special features in the treatment of superficial tumors with depth extensions ≤ 20 mm, options for wIRA-HT may include malignant melanoma (recurrences, in-transit metastases), vulvar carcinoma, skin metastases of different primary tumors, cutaneous T- and B-lymphoma, cutaneous large-area hemangiomas, inoperable squamous cell, basal cell and eccrine carcinoma. Photodynamic therapy using wIRA (e.g., in the treatment of precancerous actinic keratosis) is a further promising option in clinical oncology. wIRA may also be considered as a tool to combine HT with radio-, chemo- and immune-therapy of accessible mucosal malignancies using flexible light guides.

Acknowledgments

Phantom-based quality assurance measurements have been performed by Johannes Müller, MSc, Department of Radiation Oncology, University Hospital, Erlangen, Germany.

Disclosure statement

No potential conflict of interest was reported by the authors.

Funding

Financial support by the Dr med. h.c. Erwin Braun Foundation, Basel, Switzerland (H.P., M.N.). Peter Vaupel, Professor emeritus, is a long-standing Board Member *ad honorem* of the Dr med. h.c. Erwin Braun Foundation, Basel, Switzerland.

References

- [1] Vaupel P, Stohrer M, Krüger W, et al. Localized hyperthermia in superficial tumors using water-filtered infrared-A radiation: Evaluation of temperature distribution and tissue oxygenation in subcutaneous rat tumors. *Strahlenther Onkol.* 1991;167:353–354.
- [2] Vaupel P, Kelleher DK, Krüger W. Water-filtered infrared-A radiation: a novel technique to heat superficial tumors. *Strahlenther Onkol.* 1992;168:633–639.
- [3] Vaupel P, Kelleher DK, Krüger W. Wassergefilterte Infrarot-A-Strahlung: Eine neue Technik zur lokalen Hyperthermie oberflächlich liegender Tumoren [Water-filtered infrared-A Radiation: A novel technique for localized hyperthermia of superficial tumours]. In: Vaupel P, Krüger W, Hrsg. *Wärmetherapie mit wassergefilterter Infrarot-A-Strahlung.* Stuttgart: Hippokrates; 1992. p. 57–62.
- [4] Kelleher DK, Engel T, Vaupel P. Changes in microregional perfusion, oxygenation, ATP and lactate distribution in subcutaneous rat tumours upon water-filtered IR-A hyperthermia. *Int J Hyperthermia.* 1995;11:241–255.
- [5] Thews O, Li Y, Kelleher DK, et al. Microcirculatory functions, tissue oxygenation, microregional redox status and ATP distribution in tumors upon localized infrared-A-hyperthermia at 42 °C. *Adv Exp Med Biol.* 2003;530:237–247.
- [6] Kelleher DK, Thews O, Rzeznik J, et al. Water-filtered infrared-A radiation: a novel technique for localized hyperthermia in combination with bacteriochlorophyll-based photodynamic therapy. *Int J Hyperthermia.* 1999;15:467–474.
- [7] Kelleher DK, Thews O, Scherz A, et al. Combined hyperthermia and chlorophyll-based photodynamic therapy: tumour growth and metabolic microenvironment. *Br J Cancer.* 2003;89:2333–2339.
- [8] Kelleher DK, Bastian J, Thews O, et al. Enhanced effects of amino-laevulinic acid-based photodynamic therapy through local hyperthermia in rat tumours. *Br J Cancer.* 2003;89:405–411.
- [9] Zywietz F. Infrarot-A-Hyperthermie als strahlensensibilisierendes Agens bei Bestrahlung oberflächennah liegender Tumoren: Tierexperimentelle Untersuchungen [Infrared-A hyperthermia as a sensitizer for irradiation of superficial tumours: Animal experiments]. In: Vaupel P, Krüger W, Hrsg. *Wärmetherapie mit wassergefilterter Infrarot-A-Strahlung.* 2. Auflg. Stuttgart: Hippokrates; 1995. p. 113–26.
- [10] Morita K, Zywietz F, Kakinuma K, et al. Efficacy of doxorubicin thermosensitive liposomes (40 degrees C) and local hyperthermia on rat rhabdomyosarcoma. *Oncol Rep.* 2008;20:365–372.
- [11] Seegenschmiedt MH. Erfahrungen mit einem Infrarot-A-Hyperthermie-Projektor mit Wasserfilter zur lokal-perkutanen Hyperthermie kombiniert mit Radiotherapie bei oberflächennahen Tumoren [Experiences with water-filtered infrared-A radiation for localized, percutaneous hyperthermia combined with radiotherapy of superficial tumours]. In: Vaupel P, Krüger W, Hrsg. *Wärmetherapie mit wassergefilterter Infrarotstrahlung.* Stuttgart: Hippokrates; 1992. p. 63–76.
- [12] Seegenschmiedt MH, Klautke G, Walther E, et al. Water-filtered infrared-A-hyperthermia combined with radiotherapy for advanced and recurrent tumours. *Strahlenther Onkol.* 1996;172:475–484.
- [13] Notter M, Piazena H, Vaupel P. Hypofractionated re-irradiation of large-sized recurrent breast cancer with thermography-controlled, contact-free water-filtered infra-red-A hyperthermia: a retrospective study of 73 patients. *Int J Hyperthermia.* 2017;33:227–236.
- [14] Datta NR, Puric E, Klingbiel D, et al. Hyperthermia and radiation therapy in locoregional recurrent breast cancers: a systematic review and meta-analysis. *Int J Radiat Oncol Biol Phys.* 2016;94:1073–1087.
- [15] National Comprehensive Cancer Network (Version 1.2018). [cited 2018 Mar 20]. Available from: <https://www.nccn.org/>
- [16] ONCOLINE. [cited 2017 Dec 31]. Available from: <https://www.oncoline.nl/>
- [17] Die Arbeitsgemeinschaft Gynäkologische Onkologie (AGO). [cited 2018 Mar 10]. Available from: <https://www.ago-online.de/>
- [18] Leitlinienprogramm Onkologie. [cited 2017 Dec 31]. Available from: <https://www.leitlinienprogramm-onkologie.de>
- [19] Harms W, Budach W, Dunst J, et al. DEGRO practical guidelines for radiotherapy of breast cancer VI: therapy of locoregional breast cancer recurrences. *Strahlenther Onkol.* 2016;192:199–208.
- [20] Notter M, Münch K, Vaupel P. (2017). Re-irradiation and wIRA-hyperthermia for superficial widespread breast cancer recurrences: An update. 31. Annual Meeting of the European Society for Hyperthermic Oncology (ESHO), Athens.
- [21] Trefna HD, Crezee H, Schmidt M, et al. Quality assurance guidelines for superficial hyperthermia clinical trials: I. Clinical requirements. *Int J Hyperthermia.* 2017;33:471–482.
- [22] Dobsicek Trefna H, Crezee J, Schmidt M, et al. Quality assurance guidelines for superficial hyperthermia clinical trials : II. Technical requirements for heating devices. *Strahlenther Onkol.* 2017; 193:351–366.
- [23] Rzeznik J. Die Technik zur loko-regionalen Wärmetherapie mit wassergefilterter Infrarot-A-Strahlung [Technique for loco-regional hyperthermia with water-filtered infrared-A radiation]. In: Vaupel, P, Krüger, W., Hrsg. *Wärmetherapie mit wassergefilterter Infrarot-A-Strahlung. Grundlagen und Anwendungsmöglichkeiten.* Stuttgart: Hippokrates; 1992. p. 23–38.
- [24] CIE, No. 17.4 (1987). *International lighting vocabulary.* Vienna: International Commission on Illumination (CIE).
- [25] DIN 5031-7 (1984). *Strahlungsphysik im optischen Bereich und Lichttechnik, Teil 7: Benennung der Wellenlängenbereiche.* Berlin: Beuth.
- [26] Grote J, Süßkind R, Vaupel P. Oxygen diffusivity in tumour tissue (DS-carcinosarcoma) under temperature conditions within the range of 20–40 °C. *Pflügers Arch.* 1977;372:37–42.
- [27] Gersing E, Kelleher DK, Vaupel P. Tumour tissue monitoring during photodynamic and hyperthermic treatment using bioimpedance spectroscopy. *Physiol Meas.* 2003;24:625–637.
- [28] Kiricuta IC, Simplaceanu V. Tissue water content and nuclear magnetic resonance in normal and tumor tissues. *Cancer Res.* 1975;35:1164–1167.

- [29] Hoffmann G. Principles and working mechanisms of water-filtered infrared-A (wIRA) in relation to wound healing. *GMS Krankenhhyg Interdiszip.* 2007;2:Doc54.
- [30] Höhn A, Hartmann P, Grune V, et al. Actual isothermal effect of water-filtered infrared A (wIRA)-irradiation. *Photochem Photobiol.* 2015;91:887–894.
- [31] Piazena H, Pittermann W, Müller W, et al. Effects of water-filtered infrared-A and of heat on cell death, inflammation, antioxidative potential and of free radical formation in viable skin – first results. *J Photochem Photobiol B.* 2014;138:347–354.
- [32] Gebbers N, Hirt-Burri N, Scaletta C, et al. Water-filtered infrared-A radiation (wIRA) is not implicated in cellular degeneration of human skin. *GMS Ger Med Sci.* 2007;5:Doc08.
- [33] Jung T, Höhn A, Piazena H, et al. Effects of water-filtered infrared A irradiation on human fibroblasts. *Free Radic Biol Med.* 2010;48:153–160.
- [34] Elbuluk N, Wang F, Tran BA, et al. Infrared irradiation differentially alters collagen metabolism in lightly and darkly pigmented human skin *in vivo*. *J Dermatol Sci.* 2016;82:212–214.
- [35] Piazena H, Kelleher DK. Effects of infrared-A irradiation on skin: discrepancies in published data highlight the need for an exact consideration of physical and photobiological laws and appropriate experimental settings. *Photochem Photobiol.* 2010;86:687–705.
- [36] Hoffmann G, Hartel M, Mercer JB. Heat for wounds – water-filtered infrared-A (wIRA) for wound healing – a review. *Ger Med Sci.* 2016;14:Doc08.
- [37] Singer D, Schröder M, Harms K. Vorteile der wassergefilterten gegenüber herkömmlicher Infrarot-Strahlung in der Neonatologie [Advantages of water filtered over conventional infrared irradiation in neonatology]. *Z Geburtshilfe Neonatol.* 2000;204:85–92.
- [38] Piazena H, Meffert H, Uebelhack R. Spectral remittance and transmittance of visible and of infrared-A radiation in human skin – comparison between *in vivo* measurements and model calculations. *Photochem Photobiol.* 2017;93:1449–1461.
- [39] Piazena H, Meffert H, Uebelhack R. Physical and photobiological basics for prophylactic and therapeutic application of infrared radiation. *Akt Dermatol.* 2014;40:335–339.
- [40] Vaupel P, Rzeznik J, Stofft E. Water-filtered infrared-A radiation versus conventional infrared radiation: temperature profiles upon loco-regional thermotherapy. *J Phys Rehab Med.* 1995;5:77–81.
- [41] Stofft E, Vaupel P. Water-filtered infrared-A radiation versus fango-paraffin pack: temperature profiles upon loco-regional thermotherapy. *Phys Rehab Kur Med.* 1996;6:7–11.
- [42] Wust P. *Thermotherapy in oncology.* Bremen: Uni-Med Science; 2017.
- [43] Vaupel P, Höckel M. Blood supply, oxygenation status and metabolic micromilieu of breast cancers: characterization and therapeutic relevance. *Int J Oncol.* 2000;17:869–879.
- [44] Vaupel P. Tumor microenvironmental physiology and its implications for radiation oncology. *Sem Radiat Oncol.* 2004;14:198–206.
- [45] Barrett KE, Barman SM, Boitano S, et al. (eds.). *Ganong's review of medical physiology.* 24th ed. NewYork: McGraw-Hill; 2012.
- [46] Dewhirst MW, Vujaskovic Z, Jones E, et al. Re-setting the biologic rationale for thermal therapy. *Int J Hyperthermia.* 2005;21:779–790.
- [47] DIN 33403-3. *Klima am Arbeitsplatz und in der Arbeitsumgebung. Teil 3: Beurteilung des Klimas im Warm- und Hitzebereich auf der Grundlage ausgewählter Klimasummenmaße.* Berlin: Beuth; 2001.
- [48] Yarmolenko PS, Moon EJ, Landon C, et al. Thresholds for thermal damage to normal tissues: an update. *Int J Hyperthermia.* 2011;27:320–343.
- [49] Hellige G. Temperaturverteilung und Eindringtiefe wassergefilterter Infrarot-A-Strahlung. In: Vaupel, P, Krüger, W. Hrsg. *Wärmetherapie mit wassergefilterter Infrarot-A-Strahlung. Grundlagen und Anwendungsmöglichkeiten.* Stuttgart: Hippokrates; 1992. p. 39–50.
- [50] Krüger W, Kelleher DK, Vaupel P. Temperaturprofile im Agarphantom und Muskelgewebe bei Erwärmung mit wassergefilterter Infrarot-A-Strahlung. In: Vaupel P, Krüger W, Hrsg. *Wärmetherapie mit wassergefilterter Infrarot-A-Strahlung. Grundlagen und Anwendungsmöglichkeiten.* Stuttgart: Hippokrates; 1992. p. 51–56.
- [51] Lualdi M, Colombo A, Farina B, et al. A phantom with tissue-like optical properties in the visible and near infrared for use in photomedicine. *Lasers Surg Med.* 2001;28:237–243.
- [52] Müller J, Hartmann J, Bert C. Infrared camera based thermometry for quality assurance of superficial hyperthermia applicators. *Phys Med Biol.* 2016;61:2646–2664.
- [53] Bakker A, Kolff MW, Holman R, et al. Thermal skin damage during reirradiation and hyperthermia is time-temperature dependent. *Int J Radiat Oncol Biol Phys.* 2017;98:392–399.
- [54] Peeken JC, Vaupel P, Combs SE. Integrating hyperthermia into modern radiation oncology: What evidence is necessary? *Front Oncol.* 2017;7:132.
- [55] Molls M, Feldmann HJ, Füller J. Oxygenation of locally advanced recurrent rectal cancer, soft tissue sarcoma and breast cancer. *Adv Exp Med Biol.* 1949;345:459–463.
- [56] Vaupel P, Briest S, Höckel M. Hypoxia in breast cancer: pathogenesis, characterization and biological/therapeutic implications. *Wien Med Wochenschr.* 2002;152:334–342.
- [57] Vaupel P, Höckel M, Mayer A. Detection and characterization of tumor hypoxia using pO₂ histography. *Antioxid Redox Signal.* 2007;9:1221–1235.
- [58] Okunieff P, Urano M, Kallinowski F, et al. Tumors growing in irradiated tissue: oxygenation, metabolic state, and pH. *Int J Radiat Oncol Biol Phys.* 1991;21:667–673.
- [59] Feldmann HJ, Molls M, Füller J, et al. Changes in oxygenation patterns of locally advanced recurrent tumors under thermoradiotherapy. *Adv Exp Med Biol.* 1994;345:479–483.